Journal of Physics: Condensed Matter

PAPER • OPEN ACCESS

# Space charge layer effects in silicon studied by *in situ* surface transport

To cite this article: Frederik Edler *et al* 2019 *J. Phys.: Condens. Matter* **31** 214001

View the article online for updates and enhancements.


## Recent citations

- Thickness-dependent electronic transport through epitaxial nontrivial Bi quantum films
Doaa Abdelbarey *et al*

- Charge-transfer transition in Au-induced quantum wires on Si(553)
Frederik Edler *et al*

- Preface: fresh perspectives on internal interfaces
J Michael Gottfried and Ulrich Höfer



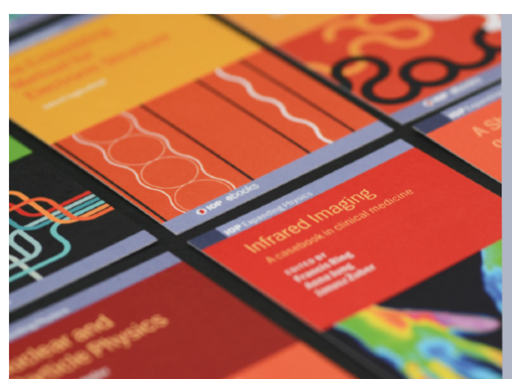

IOP ebooks™

Bringing together innovative digital publishing with leading authors from the global scientific community.

Start exploring the collection–download the first chapter of every title for free.


This content was downloaded from IP address 194.95.157.29 on 04/11/2020 at 07:43

OPEN ACCESS
IOP Publishing
Journal of Physics: Condensed Matter
J. Phys.: Condens. Matter **31** (2019) 214001 (8pp)
https://doi.org/10.1088/1361-648X/ab094e

# Space charge layer effects in silicon studied by *in situ* surface transport

**Frederik Edler[1,2], Ilio Miccoli[2], Herbert Pfnür[2,3] and Christoph Tegenkamp[1,2,3]**

[1] Institut für Physik, Technische Universität Chemnitz, Reichenhainer Str. 70, 09126 Chemnitz, Germany
[2] Institut für Festkörperphysik, Leibniz Universität Hannover, Appelstraße 2, 30167 Hannover, Germany
[3] Laboratorium für Nano- und Quantenengineering (LNQE), Leibniz Universität Hannover, Schneiderberg 39, 30167 Hannover, Germany

E-mail: christoph.tegenkamp@physik.tu-chemnitz.de

Received 17 November 2018, revised 13 February 2019
Accepted for publication 21 February 2019
Published 19 March 2019

**Abstract**
Electronic properties of low dimensional structures on surfaces can be comprehensively explored by surface transport experiments. However, the surface sensitivity of this technique to atomic structures comes along with the control of bulk related electron paths and internal interfaces. Here we analyzed the role of Schottky-barriers and space charge layers for Si-surfaces. By means of a metal submonolayer coverage deposited on vicinal Si(1 1 1), we reliably accessed subsurface transport channels via angle- and temperature-dependent *in situ* transport measurements. In particular, high temperature treatments performed under ultra high vacuum conditions led to the formation of surface-near bulk defects, e.g. SiC-interstitials. Obviously, these defects act as p-type dopants and easily overcompensate lightly n-doped Si substrates.

Keywords: space charge layer, surface transport, silicon surface

(Some figures may appear in colour only in the online journal)

## 1. Introduction

The working principle of semiconductor-based devices rely on band bending [1]. For instance, the skillful engineering of the band structure controls the efficiency and operation parameters of solar cells, rectifiers, or transistors [2]. For metal/semiconductor systems this comes inherently along with the formation of Schottky barriers, which are controlled by interface states and internal interfaces [3, 4].

This concept can be successfully applied to semiconductor surfaces, where surface states now pin the Fermi level in the system [5]. Based on the energetic positions of these states with respect to the valence band maxima and doping levels, surface states can become electronically decoupled from the bulk [6, 7]. This opens a pathway for surface transport experiments to study fundamental aspects in low dimensional electron gas systems, which are manifoldly realized by various metallic monolayer phases on Si(1 1 1) [8]. Recent examples, probed by *in situ* surface transport, are superconductivity or metal–insulator transitions in Si(1 1 1)-Pb$\sqrt{7} \times \sqrt{3}$ or Si(1 1 1)-In $4 \times 1$, respectively [9, 10].

However, there are various studies on nominally identical surface phases showing a significant variation in surface conductivities, e.g. Si(1 1 1)-$7 \times 7$ and Si(1 1 1)-Ag$\sqrt{3} \times \sqrt{3}$ reconstructions [5, 11]. To some extent these variations are explained by surface defects, e.g. physisorbates, grain boundaries within the surface phase or even substrate steps, which easily hinders the propagation of electrons. For example, the Si(1 1 1)-In $4 \times 1$-system revealed an extremely high $\sigma_{\parallel}/\sigma_{\perp}$ anisotropy ratio [7]. However, subsequent transport experiments never obtained such a high ratio again and rather showed strong variations of conductivity components [12–15]. Since systematic studies are missing to date for this system, temperature induced modifications of the Si(1 1 1) step structure may be a possible reason for this finding.

Besides the surface also the bulk properties are important. Although the potential contributions from the bulk for these systems are minimized due to Schottky barriers [6], mobile

Original content from this work may be used under the terms of the Creative Commons Attribution 3.0 licence. Any further distribution of this work must maintain attribution to the author(s) and the title of the work, journal citation and DOI.


© 2019 IOP Publishing Ltd Printed in the UK

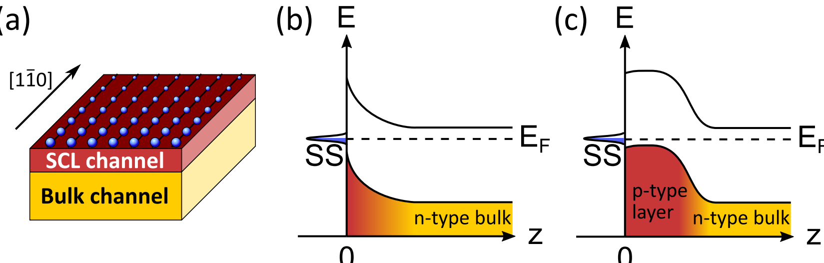


**Figure 1.** (a) A schematic of the Si(5 5 3)-Au system showing the surface reconstruction (blue dots), SCL (red) and bulk channel (yellow). (b) The energetic position of the surface state (SS) on n-type Si leads to the formation of an inversion layer. This case refers to the intrinsic SCL. (c) Band bending after p-type layer formation giving rise to a parasitic SCL contribution.

excess carriers are accumulated in the so-called space charge layer (SCL), located close to the surface, and can significantly contribute to the surface conductance [13, 16]. In case of Si, crystalline and long-range ordered surfaces, e.g. as templates for the subsequent growth of metallic adsorbates, are usually obtained by high temperature treatments in order to desorb the oxide and to enable Si surface diffusion. However, flash annealing of doped semiconductors easily leads to irreversible changes of the doping in terms of type and concentration [13, 17–20]. In particular, n-type doping was replaced by a p-type doping behavior explained either by B diffusion [18] or, more likely, C contaminations during flashing, which are resulting in interstitial defects [17]. This effect is especially distinct and effective for high flash annealing temperatures above 1150 °C [13]. Such parasitic subsurface effects change severely the contribution of the SCL and make the analysis of the surface state conductivity even more challenging.

In order to discriminate between different transport channels and to circumvent the problem of irreversible changes of the surface morphology, vicinal Si(1 1 1) surfaces with (sub) monolayer phases of metals are promising. These surfaces can provide regular and stable step arrays. Moreover, previous experiments showed that the semi-metallic character of the $(7 \times 7)$ reconstruction makes it difficult to realize stable ohmic contacts [5, 11, 21, 22]. Hence, adsorbates are helpful to provide robust surface states, a defined Fermi-level pinning and the stabilization of a well-defined vicinal surface orientation. The Si(h h k)-Au family entails these conditions. In particular, the Si(5 5 3)-Au system provides, in contrast to Si(1 1 1)-Au structures, a long-range ordered single domain structure with a surface state which is pinned 0.25 eV above the valence band maximum of Si [23]. For n-type Si a surface Schottky barrier is expected, which decouples the bulk states (figure 1(b)) [7]. However, this idealized scenario dramatically changes if the surface-near doping profile is altered, e.g. by high temperature treatments (figure 1(c)). The Si(5 5 3)-Au system provides metallic 1D surface states only along the $[1\,\bar{1}\,0]$ direction [23–26]. This at first will enable us to characterize the SCL by evaluating the conductivity $\sigma_\perp$ measured perpendicular to the step direction.

In this paper we performed four point-probe (4PP) *in situ* transport measurements on Si(5 5 3)-Au. The gradual rotation of a squared tip configuration allowed us to deduce the conductivity components both along and perpendicular to the wires and, hence, to measure accurately the conductivity of the SCL. Using both heavily and lightly doped Si samples, we studied systematically the influence of high temperature annealing steps towards the modification of surface-near doping profiles. The modeling of temperature-dependent transport measurements showed that upon annealing, even under ultra-high vacuum conditions, parasitic p-type doping occurs with dopant concentrations up to $10^{16}$ cm$^{-3}$ within a surface-near region of 1 $\mu$m deep.

## 2. Experimental setup

The experiments were performed using lightly and heavily n-type doped (phosphorus) Si(5 5 3) crystals with a nominal bulk resistivity of $\rho = 1700$ $\Omega$cm ($N_D \approx 3 \times 10^{12}$ cm$^{-3}$) and $\rho = 0.015$ $\Omega$cm ($N_D \approx 2 \times 10^{18}$ cm$^{-3}$), respectively. The crystals were cut into samples of $1 \times 0.5$ cm$^2$ size and cleaned sequentially using acetone, isopropyl alcohol as well as deionized water in an ultrasonic bath. To ensure low pressures during sample preparation, the samples were carefully degassed in an ultrahigh-vacuum (UHV) chamber operated at a base pressure of $1 \times 10^{-10}$ mbar for several hours by direct-current heating at 700 °C. Au atomic chains were prepared as follows: in a first step, the samples were flash annealed several times (see discussion in section 3) at 1150 °C for a few seconds (2–3 s) while the pressure was always kept below $1 \times 10^{-9}$ mbar. Afterwards, 0.48 ML of Au was evaporated at 650 °C using a flux-controlled *e*-beam evaporator to realize stable ohmic contacts.

The overall quality of the sample preparation was controlled by high-resolution low-energy electron diffraction (SPA-LEED, see figures 2(a) and (b)). The spot splitting along the $[1\,1\,\bar{2}]$-direction as well as the $\times$2-streaks along the $[1\,\bar{1}\,0]$-direction evidence the formation of long-range ordered single domain chain structures on Si(5 5 3). More details can be found in [27]. The transport properties of the Au chains were analyzed in the same UHV chamber by means of a 4PP setup consisting of scanning electron microscope (SEM) and four independently operating scanning tunneling microscope (STM) scanners, each equipped with NaOH-etched W tip [28]. The SEM is used for a precise positioning of the tips. In particular, the squared tip configuration was used in this study as it allows measuring independently the two transport components ($\sigma_\parallel$ and $\sigma_\perp$) within the plane. For more details the reader is referred to [29]. Temperature dependent 4PP measurements between 40–300 K

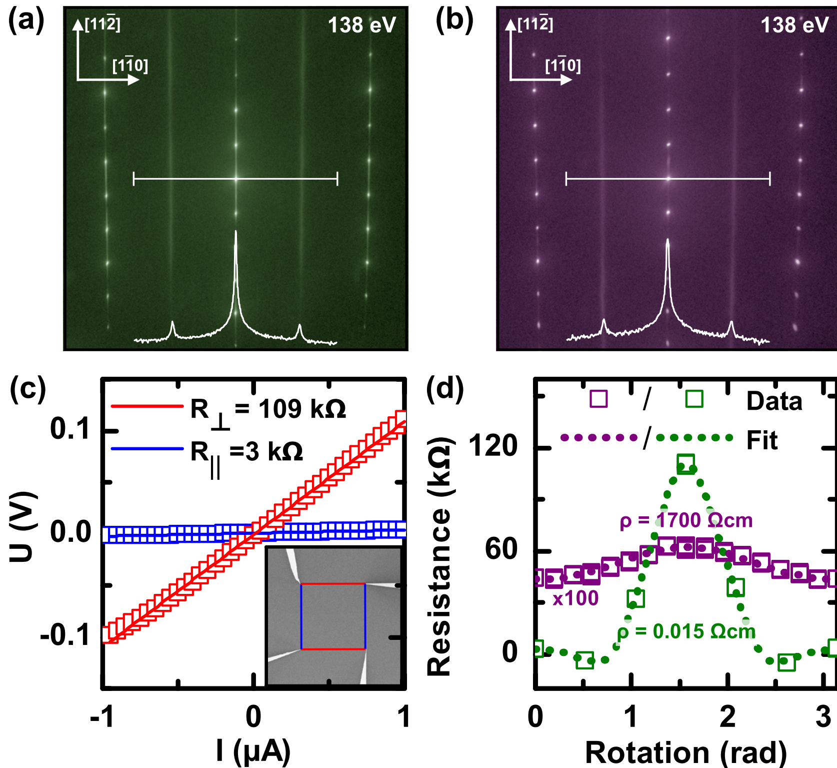


**Figure 2.** (a) and (b) SPA-LEED patterns of single domains of Au adsorbed on high- (a) and low-doped (b) Si(5 5 3) samples. (c) $I(V)$ curves obtained for a squared probe geometry on Si(5 5 3)-Au ($\rho = 0.015$ Ωcm), where the current is probed along the parallel (blue) and perpendicular direction (red) to the chains. The inset shows the squared assembly of the tips with a tip distance of 75 $\mu$m. (d) Resistances measured for various angles by using the rotational square method done on the same surface reconstruction, but on differently doped Si-samples ($\rho = 1700$ Ωcm (purple) and $\rho = 0.015$ Ωcm (green)). $\pi/2$ corresponds to a current along the perpendicular direction. All measurements were performed at room temperature. Both surfaces were flash annealed five times before Au adsorption.

were performed using ℓHe flow cryostat. The temperature was measured with a Pt100 resistance mounted on the sample stage.

## 3. Results and discussion

### *3.1. In situ measurement of the space-charge layer*

Figure 2(c) shows $I(V)$-curves obtained on Si(5 5 3)-Au measured in a square 4PP geometry on a sample with a nominal bulk resistivity of $\rho = 0.015$ Ωcm. The probe spacing for all measurements was 75 $\mu$m. Here, $R_{\|}$ corresponds to a current injected along the $[1\,\bar{1}\,0]$-direction, i.e. parallel to the atomic wires, while for $R_{\perp}$ along the $[1\,1\,\bar{2}]$-direction. Clearly, we can distinguish two different slopes and the corresponding resistances are $R_{\|} = 3$ kΩ and $R_{\perp} = 109$ kΩ, respectively. The conductivities can be deduced with high precision from the angular dependence of the anisotropic resistance values by the so-called rotational square method [29]. The dotted green line in figure 2(d) is the best fit to the data obtained on Au/Si(5 5 3) sample with $\rho = 0.015$ Ωcm and reveals conductivities of $\sigma_{\|} = 15$ $\mu$S/□ along the chains and $\sigma_{\perp} = 0.97$ $\mu$S/□ in the perpendicular direction, respectively. The anisotropy for this system is around 15.

As explained in detail in the introduction, the conductivity $\sigma_{\perp}$ is not triggered by the surface state band structure and must be related to transport across the Si-bulk, i.e. the SCL. We will show below, that the thickness of this bulk channel is smaller than the probe spacing, thus the rotational square method for 2D electron gas systems is applicable and measures both the anisotropic surface and isotropic bulk channels. Indeed, the LEED image (see figure 2(a)) revealed long range ordered wire structures. Therefore, we assume that hopping via surface defect states is not dominating in our transport experiments.

We prepared the same surface reconstruction on nominally lightly doped samples ($\rho = 1700$ Ωcm, see figure 2(b)), which underwent also five flash annealing cycles. The corresponding rotational square measurement is shown in panel (d) as well. Apparently, the absolute resistances strongly differ compared to the previous case [15, 26, 30, 31]. The analysis reveals conductivities of $\sigma_{\|} = 239$ $\mu$S/□ and $\sigma_{\perp} = 186$ $\mu$S/□. Albeit the surface structure is similar, the conductivity ratio is lowered by one order of magnitude. Hence, the surface transport experiment is extremely sensitive to the concentration of the bulk dopants.

Our conductivity measurements together with results of a former study performed on samples with an intermediate doping ($\rho = 1$–10 Ωcm) are summarized in figure 3(a) [15, 30, 31]. There is a clear correlation between the conductivities and the bulk dopant concentrations. Moreover, also the ratio, $\sigma_{\|}/\sigma_{\perp}$, depends on the initial dopant concentration as

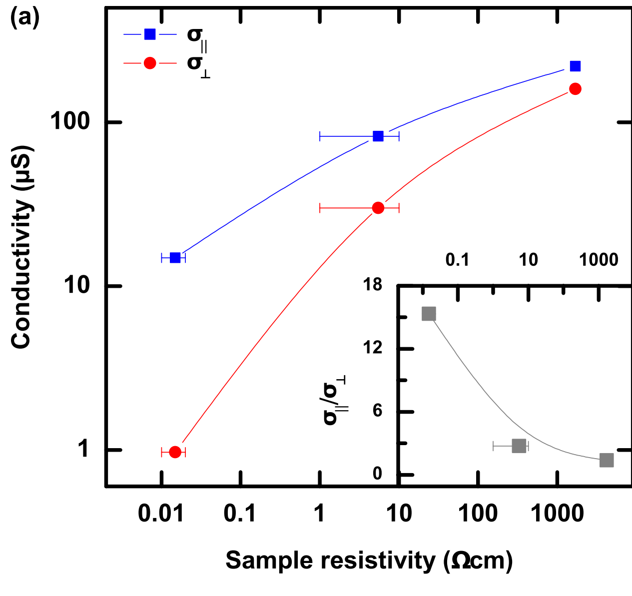


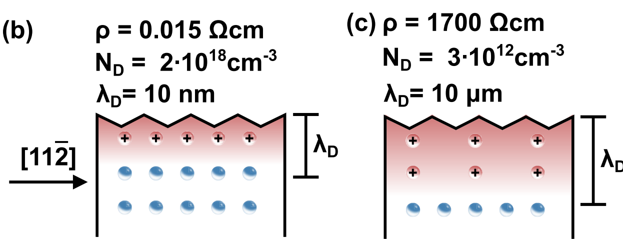


**Figure 3.** (a) Conductivity components measured parallel ($\sigma_{\|}$) and perpendicular ($\sigma_{\perp}$) to the Au atomic chains on Si(5 5 3) at 300 K on samples with $\rho = 0.015$ Ωcm, $\rho$ =1–10 Ωcm (data from [31]) and $\rho = 1700$ Ωcm. The inset shows the anisotropy ratios as a function of the sample resistivity. The lines are a guide to the eyes. (b) and (c) Schematic drawing of the space-charge layer illustrating the different dopant concentrations $N_D$ and Debye lengths $\lambda_D$.

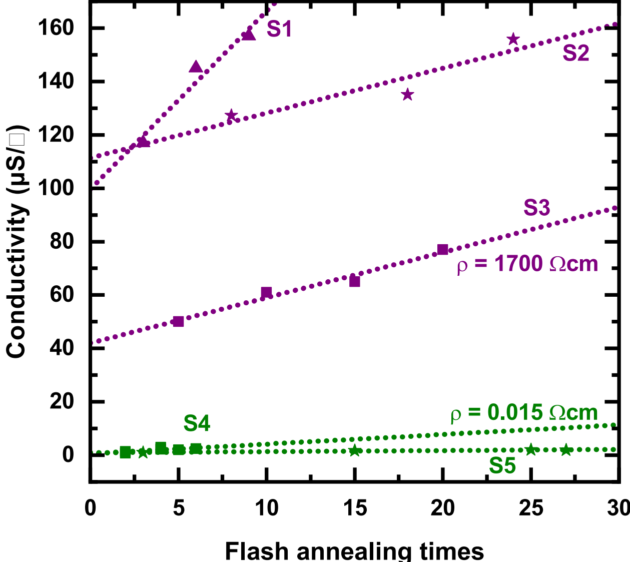


**Figure 4.** Conductivity ($\sigma_{\perp}$) measured along the $[1\,1\,\bar{2}]$-direction at 300 K as a function of the flash annealing cycles. Different symbols refer to different samples (S1–S5). The dotted lines are fits to the data.

shown by the inset. Surprisingly, the higher the dopant concentration, the lower the conductivities and the higher the anisotropy between the parallel and perpendicular direction.

Qualitatively, the dependence of the conductivity components on the bulk resistivity can be rationalized taking into account the expansion of the SCL which forms beneath the Si-surface due to Fermi-level pinning of the surface states: from the position of the surface state with respect to the valence band maximum the band bending is around $\Phi \approx 0.8$ eV [23]. This Schottky barrier decouples effectively the Si-bulk from the surface transport channels, which we only access by our nanoprobes [7]. Assuming a homogeneous dopant distribution in silicon ($\epsilon = 11.7$) the Debye lengths $\lambda_D \approx \sqrt{\epsilon\epsilon_0\Phi/N_D e^2}$ for the low- ($N_D \approx 3 \times 10^{12}$ cm$^{-3}$) and high-doped ($N_D \approx 2 \times 10^{18}$ cm$^{-3}$) samples for this idealized scenario are in the order of 10 $\mu$m and 10 nm, respectively [32]. Thus, in heavily doped Si-samples the bulk charge carriers are confined in a very small near-surface area as schematically depicted in figure 3(b) and the high resistances are explained by the high concentration of ionized bulk donors in this area. The detailed calculation of the carrier concentrations within the SCL revealed that mainly holes are contributing. Moreover, the strongly confined holes experience also the step structure of the vicinal Si-surface resulting in a high anisotropy. The conductivity measured along the Si-steps is not affected by the surface step structure. As obvious from figure 3(a) the conductivity decreases by one order of magnitude when the dopant concentration changes by 5 orders of magnitude. This is in good agreement with quantum-mechanical based numerical simulation of the electron mobility in Si at room temperature [33]. Therefore, lightly doped samples should result in a better SCL performance (see figure 3(c)). However, these surfaces are extremely prone to changes of the dopant concentration and distribution upon *in situ* sample preparation, as we will show in the following. Regarding the contribution of the surface state to the conductivity, we assume that the filling factors do not severely change as a function of the bulk doping concentration, so that the surface state conductivity along the steps is on average the same for all samples. We will show below that quantitative description based on a simple Schottky model is feasible.

### 3.2. *Effect of flash annealing*

As mentioned, the surface-near area in semiconductors easily degrade upon high temperature annealing. For a systematic approach towards these modifications, we studied the change of the SCL contribution as a function of the flash annealing time. Figure 4 summarizes $\sigma_{\perp}$ measured in the direction perpendicular to the Au-chains for five different samples. The conductivities were measured after each step of preparation using the above mentioned rotational square method. Lightly doped samples are much more susceptible to high temperature *in situ* flash annealing cycles compared to high-doped samples. The increase of the conductivity for the lightly doped samples on average is 3.3 $\mu$S/□ per annealing step while for high-doped samples the change is almost negligible (0.2 $\mu$S/□ per flash). Obviously, the formation of a parasitic

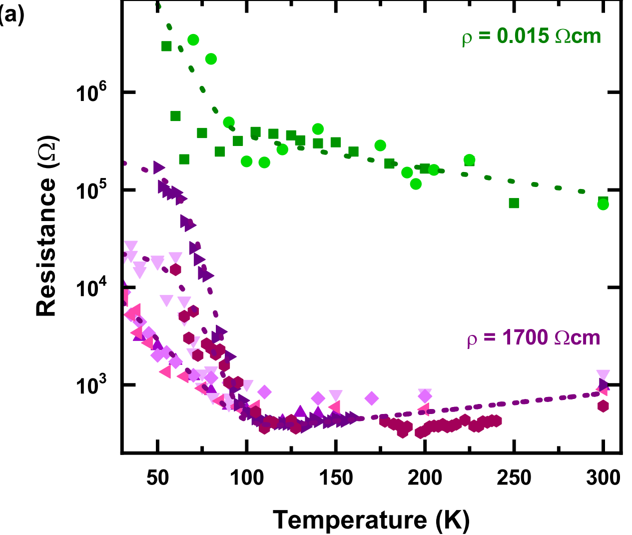


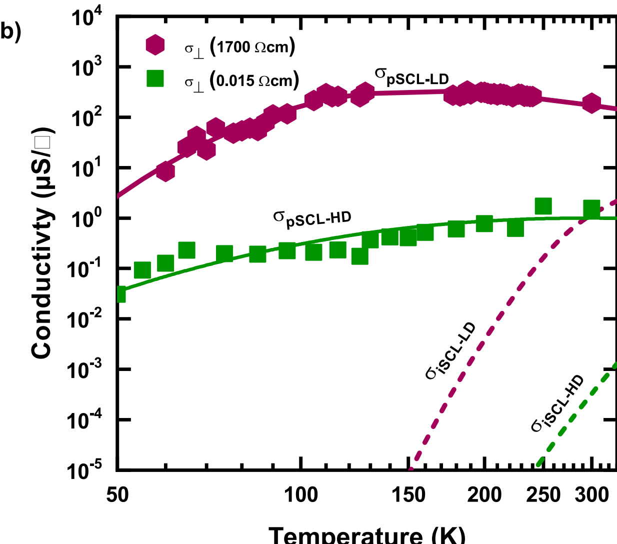


**Figure 5.** (a) Temperature dependence of the resistance $R_\perp$ of eight different Si(5 5 3)-Au samples. Notably, all data sets see a drastic change of resistance occurring at around 100–110 K. (b) Conductivity measured perpendicular to the wire direction plotted exemplarly for two circles data sets from (a). While the conductivity can not be explained by a model of an intrinsic SCL for both low- (LD) and high-doped (HD) sample (dashed lines), a parasitically formed p-type layer beneath the surface reasonably explain the conductivity (solid lines).

p-type layer (see below) upon annealing cannot overcompensate our high-doped samples. From this we can already conclude that the parasitic dopant concentration is small compared to $N_\mathrm{D} = 2 \times 10^{18}$ cm$^{-3}$.

In order to quantify the conductivity with respect to the doping concentration and doping profile we performed temperature dependent transport experiments between 50–300 K. Figure 5(a) shows the resistance component $R_\perp$ measured along the $[1\,1\,\bar{2}]$-direction on eight different samples (six samples with $\rho = 1700$ Ωcm and two with $\rho = 0.015$ Ω cm). The direction perpendicular to the chains is not strongly influenced by the details of the surface states [23–25]. Notably, all datasets show at around 100 K for $R_\perp$ an increases by 2–3 orders of magnitude. The difference of the absolute values for the high- and low-doped samples was discussed already in context of figure 3(a).

Although the solubility of Au in Si is not negligible [34], the adsorbate itself is not inducing this effect for the following reasons: first of all, Au is known to form deep level traps at around 300 meV above the valence band edge of Si. Any significant contribution of Au should have result in an activated transport signal at higher temperatures. Secondly, Au-adsorption after each high temperature annealing step as well as at the end of these steps revealed similar results. Moreover, a similar degradation mechanism in Si(1 1 1) was observed in the course of surface transport experiments with In-submonolayers [13]. Therefore, we exclude that the Au-submonolayer is responsible for the formation of a parasitic transport background.

### *3.3. Modeling of transport data*

For a quantitative description, various conduction channels are contributing. The total conductivity in our case is the sum of transport from the surface ($\sigma_S$), the bulk ($\sigma_B$), and the surface near area ($\sigma_\mathrm{SCL}$). Thereby, the charge carriers can be transmitted via hopping or band conductivity. As outlined above, for the Au(5 5 3) system we can assume $\sigma_S \approx 0$ along the $[\bar{1}\,\bar{1}\,2]$-direction, i.e. perpendicular to the direction of the wires, in view of electronic bands, that were found only along the wires around $E_\mathrm{F}$, and a low surface defect concentration. Similarly to the In/Si(1 1 1) system, the intrinsic p-type SCL (inversion layer) in case of a n-type Si is electrically decoupled from the bulk and penetration of current into the bulk can be ignored ($\sigma_B = 0$), thus only the SCL should contribute [6, 7]. Due to the long-rage order of the surface structure and the low bulk defect-concentration of the Si wafers, hopping is only of minor importance for the following discussion. Details about the calculation of the band conductivity of the SCL are outlined in the appendix.

We will show in the following, that an intrinsic SCL (iSCL) contribution cannot explain the experimental findings. Instead, a parasitic SCL (pSCL), which results obviously from high temperature treatments in vacuum, is dominating. While for the pristine n-type Si surface the Schottky barrier is located at the surface, it shifts towards the location of the pn-junction that is formed upon the flash-annealing induced modification of the surface (see figure 1(c)). Although for both types of SCL channels the transport is mainly mediated by holes, the carriers refer to a minority and majority charges for the intrinsic n-type and parasitic p-type doping, respectively.

For instance, figure 5(b) shows two conductivity curves measured on a lightly and a heavily doped Si sample. As obvious, a description of the data based on iSCL (dashed lines) fails entirely for both heavily and lightly doped samples. Thereby, the minority concentration $p$ and hole mobility $\mu_\mathrm{p}$ for the iSCL were calculated solving the Poisson equation and using empirically derived models [35, 36]. For further details we refer to the appendix.

A reasonable modeling of our data is obtained yet for both nominally heavily and lightly doped samples if p-type dopants with an ionization energy of $E_\mathrm{A} \approx 45$ meV are assumed.

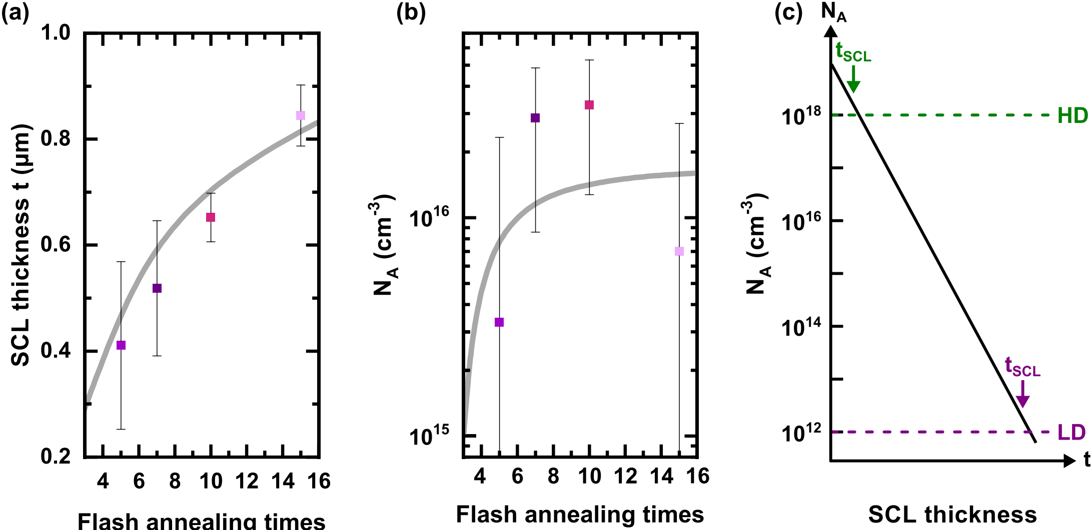


**Figure 6.** Calculated doping SCL thickness $t$ (a) and doping $N_A$ (b) as a function of the total flash annealing times for the low-doped samples. the color code corresponds to the data sets shown in figure 5(a). The grey lines are guides to the eye. (c) Schematic showing the exponentially decaying $N_A$ concentration into the bulk. The dashed lines denote the intrinsic doping levels (LD and HD). The thickness of the SCL ($t_{SCL}$) is indicated. For details see text.

Thereby, we assume an exponentially decaying parasitic profile into the bulk (see appendix). For the high-doped sample the fit reveals a doping concentration in the order of $N_A = 1 \times 10^{18}$ cm$^{-3}$ with a SCL thickness $t$ of around 1 nm. This thickness is close to the nominal Debye length which we estimated before, thus heavily doped samples are only marginally affected by our flash-annealing cycles. Strictly speaking, also the iSCL, which is located at the inner pn-junction, should be considered. However, this contribution is smaller by at least 2 orders of magnitude (see green dashed line in figure 5(b)) and can be neglected at this point. For the case of the lightly doped samples, the best fit to the data is obtained for an acceptor concentration in the order of $N_A = 5 \times 10^{16}$ cm$^{-3}$ and a SCL thickness $t \approx 0.5$ $\mu$m, again with an ionization energy of around $E_A = 45$ meV. Nonetheless, the ionization energies found for the low-doped samples vary between 45–70 meV and may be indicative for interstitial carbon defects rather substitutional doping with B [17].

Apparently, upon annealing the initial doping concentration of the lightly doped sample is changed by three orders of magnitude to the high temperature annealing steps in UHV, thus overcompensating the initial dopant profile. It should be noted that the sheet equivalent of this C-induced acceptor concentration is as low as $10^{10}$ cm$^{-2}$, i.e. heating the sample at 1150 °C for only 1 s at $1 \times 10^{-9}$ mbar can easily cause such a contamination (assuming a sticking coefficient of 1). Also, the concentrations found are well-below the solubility limit of C in solid Si. With an enthalpy of roughly 2.3 eV/atom the solubility at the high temperatures is still as high as $10^{24}$ cm$^{-3}$ [37].

All data sets shown in figure 5(a) were analyzed in detail with the above mentioned model. Figure 6 summarizes the dependence of $N_A$ and $t$ from the flash annealing cycles for the lightly doped samples. Albeit the error bars are quite large, there is general trend that under our conditions the thickness of the new parasitic p-type layer is around 1 $\mu$m. This thickness might be surprising at first sight, but is in line with carbon diffusion experiments in silicon [38]. Particularly, for interstitial C in Si the activation energy is around 0.87 eV [39]. With a reported diffusion prefactor of 0.44 cm$^2$ s$^{-1}$, easily diffusion lengths in the $\mu$m-range are obtained. For the high-doped sample, the SiC interstitials also should diffuse by around 1 $\mu$m into the bulk. Of course, for higher and longer flash annealing temperatures and a worse vacuum, the thickness $t$ and dopant concentration $N_A$ should further increase. However, it seems experimentally almost impossible to reduce these numbers significantly.

Figure 6(c) shows a schematic of the exponentially decaying acceptor concentration into the bulk. The dashed (horizontal) lines denote the donor concentrations for the high-doped and low-doped Si-samples. As obvious, the $N_A$ doping profile intersects these intrinsic levels at different depths giving rise to different parasitic SCL thicknesses. At least, where the acceptor concentration is large compared to the donor concentrations, overcompensation takes place. Up to this depth, the band structure is changed as sketched in figure 1(c). This qualitatively explains, why the SCL-thickness differ for heavily and lightly doped samples, while the acceptor profile itself, induced by high temperature annealing, should not depend on the pristine doping concentrations.

## 4. Summary and conclusion

In summary, we analyzed in detail the SCL conductivity on vicinal Si(1 1 1), coated with 0.48 ML of Au, as function of high temperature *in situ* annealing steps. Using angle- and temperature-dependent 4PP-measurements, the conductivity component across the wire direction was reliably measured and correlated with the transport along the space charge layer channel. Even under extremely clean conditions, this internal interface is altered. Parasitic surface-near doping due to SiC-interstitials occurred with typical concentrations in the order

of $10^{15}$–$10^{16}$ cm$^{-3}$. Therefore, in particular lightly doped Si samples seem to be prone to this effect upon high temperature treatment.

Intuitively, lightly doped Si samples for surface sensitive transport measurements are used. Our results clearly revealed, that these samples are extremely sensitive. Therefore, moderately doped samples are more suitable. Lowering the flash temperatures will reduce the parasitic doping effect [13], but at the expense of less ordered surfaces. A way out of this dilemma might be homoepitaxial growth at step flow conditions of around 700 °C for future transport experiments [40]. We showed that our experimental findings can be satisfactorily described by means of a simple band bending model. Changes of the electrochemical potential at the surface state induced by variations of bulk doping were not considered. We expect that these effects are small, but any systematic investigation of such effects requires an even better control of the interfaces than what could be achieved here.

## Acknowledgment

Financial support by the Deutsche Forschungsgemeinschaft (DFG) through the Research Unit FOR1700 (Te386/10-2 and Te386/9-1) is gratefully acknowledged.

## Appendix

As sketched in figure 1(a) the Si(553)-Au system provides several transport paths (surface, SCL and bulk). However, atomic Au wires grown on n-type Si(553) surfaces provide a Schottky barrier and no dispersing surface states long the $[\bar{1}\bar{1}2]$-direction. Therefore, we have direct access to the space charge layer (SCL). According to ARPES measurements, the valence band maximum is around 0.25 eV below the Fermi level [23]. Besides the SCL contribution, which is a result of the Fermi-level pinning of the surface states giving rise to an inversion layer, we also consider a SCL-like transport channel, which is formed upon high temperature treatment of the surface and which mimics rather a p-type doped layer. We term the two types intrinsic (iSCL, figure 1(b)) and parasitic SCL (pSCL, figure 1(c)). In contrast to iSCL, the transport is mediated by majority charge carriers for the pSCL. In the following we will briefly sketch how these different contributions were calculated. The results are discussed in context of figure 4(b).

### *A.1. Intrinsic SCL (iSCL)*

Depending on the Fermi level at the surface and type of the surface states (acceptors or donors), electrons are transfered from the bulk into the surface states which are screened by an equivalent space charge within the semiconductor resulting in an intrinsic formation of a SCL.

This SCL distribution is described by solving the Poisson's equation

$$\frac{\mathrm{d}^2\Phi(z)}{\mathrm{d}z^2} = -\frac{\rho(z)}{\epsilon}, \tag{A.1}$$

where $\Phi(z)$ is the potential variation, i.e. the band bending of the SCL, $\epsilon$ the dielectric constant of Si and $\rho(z)$ the charge density, which depends on the density of ionized acceptors $N_\mathrm{A}$ and donors $N_\mathrm{D}$, as well as the concentration of the electrons $n(z)$ and holes $p(z)$, respectively:

$$\rho(z) = e(N_\mathrm{D} - N_\mathrm{A} + p(z) - n(z)). \tag{A.2}$$

It is convenient to define the dimensionless potential $u$

$$u(z) = e\Phi(z)/(k_\mathrm{B}T) = E_\mathrm{F} - E_\mathrm{i}(z)/(k_\mathrm{B}T). \tag{A.3}$$

Here $E_\mathrm{i}(z)$ is the $z$-dependent position of the bulk midgap energy.

Following the arguments given in the review article by Hasegawa *et al* [8], the accumulation of the excess charge, i.e. hole and electron concentrations across the SCL interface for the case of a n-type Si material can be calculated via

$$\Delta p = \int_0^\infty [p(z) - N_\mathrm{A}]\mathrm{d}z \tag{A.4}$$

and

$$\Delta n = \int_0^\infty [n(z) - N_\mathrm{D}]\mathrm{d}z, \tag{A.5}$$

where $p(z) = n_\mathrm{i}\exp(-u(z))$ and $n(z) = n_\mathrm{i}\exp(u(z))$ denote the hole and electron concentrations across the interface. $n_\mathrm{i}$ is the intrinsic carrier concentration

$$n_\mathrm{i} = 2\left(\frac{m^* k_\mathrm{B}T}{2\pi\hbar^2}\right)^{3/2}\exp(-E_\mathrm{g}/2k_\mathrm{B}T) \tag{A.6}$$

with the band gap energy $E_\mathrm{g}$.

The mobilities $\mu_\mathrm{p}$ and $\mu_\mathrm{n}$ of the excess carrier concentrations are also a function of the temperature $T$. Moreover, the mobility is limited by phonon- and impurity-scattering. Based on results by [35, 36, 41, 42] the temperature dependent mobility (in units cm$^2$/(Vs)) in our case for a given donor concentration $N_\mathrm{D}$ is approximated by ($T$ and $N_\mathrm{D}$ in units of K and cm$^{-3}$, respectively) [35]:

$$\mu_\mathrm{p}(T, N_\mathrm{D}) = 54.3(T/300)^{-0.57} + \frac{1.36\times10^8 T^{-2.23}}{1 + [N_\mathrm{D}/(2.35\times10^{17}(T/300)^{2.4})]0.88(T/300)^{-0.146}} \tag{A.7}$$

and

$$\mu_\mathrm{e}(T, N_\mathrm{D}) = 88(T/300)^{-0.57} + \frac{7.4\times10^8 T^{-2.33}}{1 + [N_\mathrm{D}/(1.26\times10^{17}(T/300)^{2.4})]0.88(T/300)^{-0.146}}. \tag{A.8}$$

These mobilities of the carriers are bulk drift mobilities and provide a correct description for carriers close to the surface if specular scattering is assumed [16]. Finally, the temperature dependent SCL-conductivity was calculated using Mathematica [43] via

$$\sigma_\mathrm{SCL} = e(\mu_\mathrm{p}\Delta p + \mu_\mathrm{n}\Delta n). \tag{A.9}$$

The results for a n-type Si material with a resistivity of $\rho = 1700\ \Omega$cm is shown in figure 5(b). At room temperature this value well below 1 $\mu$S.

### *A.2. Parasitic sub-surface p-type SCL (pSCL)*

High temperature annealing of Si-surfaces causes irreversible changes of the surface near doping profile. Apparently, acceptors are introduced from the surface and their concentration is assumed to decay exponentially towards the bulk, i.e. $N_A(t) = N_A \exp(-t/\lambda)$), where $N_A$ denote the concentration at the surface ($t = 0$). The hole concentration, i.e. ionized acceptor density as a function of the SCL thickness $t$ was calculated via [36]

$$p(T, N_A, t) = \frac{N_A(t)}{1 + \left[4 + 2\exp\left(-\frac{E_A}{k_B T}\right)\right]\exp\left(\frac{E_A - E_F}{k_B T}\right)}, \quad \text{(A.10)}$$

where $E_A$ is the acceptor energy. As shown, the concentration of parasitic acceptor states is at maximum $10^{18}$ cm$^{-3}$, thus the dependency of the ionization energy on the acceptor concentration was neglected in our calculations [36].

In order to capture the depth distribution of the acceptor states, which give rise to hole majority charge carriers, the sheet conductivity is obtained by integration of the SCL thickness:

$$\sigma_{\mathrm{SCL},\square} = e \int_0^{\infty} \mu_p(T, t, N_A)\, p(T, t, N_A)\mathrm{d}t. \quad \text{(A.11)}$$

Again, from fitting temperature dependence of the pSCL conductivity, using Mathematica [43], we deduced the decay constant $\lambda$ and doping concentration $N_A$. Thereby, the space charge layer thickness can be identified with the decay constant ($t_{SCL} = \lambda$), if the acceptor concentration is large compared to the intrinsic n-type concentration $N_D$. For this scenario, overcompensation by the parasitic acceptors takes place. Besides the exponentially decaying profile, we modeled also homogeneous as well as triangularly shaped profiles which all gave qualitatively the same findings (within 20%).

## ORCID iDs

Herbert Pfnür https://orcid.org/0000-0003-1568-4209
Christoph Tegenkamp https://orcid.org/0000-0003-0453-0765

## References

[1] Krömer H 2001 *Rev. Mod. Phys.* **73** 783
[2] Bardeen J and Brattain W H 1948 *Phys. Rev.* **74** 230–1
[3] Heine V 1965 *Phys. Rev.* **138** A1689–96
[4] McLean A B and Williams R H 1988 *J. Phys. C: Solid State Phys.* **21** 783
[5] Wells J W, Kallehauge J F, Hansen T M and Hofmann P 2006 *Phys. Rev. Lett.* **97** 206803
[6] Mayer J W, Marsh O J, Shifrin G A and Baron R 1969 *Can. J. Phys.* **45** 4073
[7] Kanagawa T, Hobara R, Matsuda I, Tanikawa T, Natori A and Hasegawa S 2003 *Phys. Rev. Lett.* **91** 036805
[8] Hasegawa S, Tong X, Takeda S, Sato N and Nagao T 1999 *Prog. Surf. Sci.* **60** 89–257
[9] Zhang T *et al* 2010 *Nat. Phys.* **6** 104
[10] Frigge T *et al* 2017 *Nature* **544** 207
[11] Hofmann P and Wells J W 2009 *J. Phys.: Condens. Matter* **21** 013003
[12] Hasegawa S 2007 *Chin. J. Phys.* **45** 385
[13] Uetake T, Hirahara T, Ueda Y, Nagamura N, Hobara R and Hasegawa S 2012 *Phys. Rev.* B **86** 035325
[14] Edler F, Miccoli I, Demuth S, Pfnür H, Wippermann S, Lücke A, Schmidt W G and Tegenkamp C 2015 *Phys. Rev.* B **92** 085426
[15] Okino H, Matsuda I, Hobara R, Hasegawa S, Kim Y and Lee G 2007 *Phys. Rev.* B **76** 195418
[16] Yoo K and Weitering H H 2002 *Phys. Rev.* B **65** 115424
[17] Zhang H M, Sakamoto K, Hansson G V and Uhrberg R I G 2008 *Phys. Rev.* B **78** 035318
[18] Liehr M, Renier M, Wachnik R A and Scilla G S 1987 *J. Appl. Phys.* **61** 4619–25
[19] Hirahara T, Matsuda I, Liu C, Hobara R, Yoshimoto S and Hasegawa S 2006 *Phys. Rev.* B **73** 235332
[20] Bruns D, Gevers S and Wollschläger J 2011 *Surf. Sci.* **605** 861–7
[21] Heike S, Watanabe S, Wada Y and Hashizume T 1998 *Phys. Rev. Lett.* **81** 890–3
[22] Tanikawa T, Yoo K, Matsuda I, Hasegawa S and Hasegawa Y 2003 *Phys. Rev.* B **68** 113303
[23] Crain J N, McChesney J L, Zheng F, Gallagher M C, Snijders P C, Bissen M, Gundelach C, Erwin S C and Himpsel F J 2004 *Phys. Rev.* B **69** 125401
[24] Crain J N, Kirakosian A, Altmann K N, Bromberger C, Erwin S C, McChesney J L, Lin J L and Himpsel F J 2003 *Phys. Rev. Lett.* **90** 176805
[25] Crain J N and Pierce D T 2005 *Science* **307** 703–6
[26] Edler F, Miccoli I, Stöckmann J P, Pfnür H, Braun C, Neufeld S, Sanna S, Schmidt W G and Tegenkamp C 2017 *Phys. Rev.* B **95** 125409
[27] Hafke B, Frigge T, Witte T, Krenzer B, Aulbach J, Schäfer J, Claessen R, Erwin S C and von Hoegen M H 2016 *Phys. Rev.* B **94** 161403(R)
[28] Ibe J P, Bey P P Jr, Brandow S L, Brizzolara R A, Burnham N A, DiLella D P, Lee K P, Marrian C R K and Colton R J 1990 *J. Vac. Sci. Technol.* A **8** 3570–5
[29] Miccoli I, Edler F, Pfnür H and Tegenkamp C 2015 *J. Phys.: Condens. Matter* **27** 223201
[30] Okino H, Hobara R, Matsuda I, Kanagawa T, Hasegawa S, Okabayashi J, Toyoda S, Oshima M and Ono K 2004 *Phys. Rev.* B **70** 113404
[31] Okino H, Matsuda I, Yamazaki S, Hobara R and Hasegawa S 2007 *Phys. Rev.* B **76** 035424
[32] Mönch W 2001 *Semiconductor Surfaces and Interfaces* (Berlin: Springer)
[33] Pozdnyakov D 2014 *J. Comput. Electron.* **13** 338–51
[34] Stolwijk N, Schuster B, Hölzl J, Mehrer H and Frank W 1983 *Physica B + C* **116** 335–42
[35] Arora N, Hauser J and Roulston D 1982 *IEEE Trans. Electron Devices* **29** 292–5
[36] Li S S 1978 *Solid-State Electron.* **21** 1109–17
[37] Durand F and Duby J C 1999 *J. Phase Equilib.* **20** 61
[38] Werner A, Gossmann H J, Jacobson D and Gösele U 1998 *Appl. Phys. Lett.* **73** 2465
[39] Tipping A and Newman R 1987 *Semicond. Sci. Technol.* **2** 315
[40] Ichimiya A, Nakahara H, Hashizume T and Sakurai T 1993 *Surf. Sci.* **298** 284–92
[41] Long D 1960 *Phys. Rev.* **120** 2024–32
[42] Norton P, Braggins T and Levinstein H 1973 *Phys. Rev.* B **8** 5632–53
[43] Wolfram Research Inc. 2014 *Mathematica 10.0* (Champaign, IL: Wolfram Research Inc.) (www.wolfram.com)